Microporous and Mesoporous Materials 198 (2014) 55–62

Contents lists available at ScienceDirect

Microporous and Mesoporous Materials

journal homepage: www.elsevier.com/locate/micromeso

Ion-exchange resin modified with aggregated nanoparticles of zirconium hydrophosphate. Morphology and functional properties

Yuliya S. Dzyazko [a,*], Ludmila N. Ponomaryova [a], Yurii M. Volfkovich [b], Vladimir V. Trachevskii [c], Alexey V. Palchik [a]

[a] V.I. Vernadskii Institute of General and Inorganic Chemistry of the National Academy of Science of Ukraine, Palladin Ave. 32/34, 03680 Kiev, Ukraine
[b] A.N. Frumkin Institute of Physical Chemistry and Electrochemistry of the Russian Academy of Science, Leniskii Pr. 31, 119071 Moscow, Russian Federation
[c] G.V. Kurdyumov Institute of Metal Physics of the National Academy of Science of Ukraine, Acad. Vernadskii Ave. 36, 03680 Kiev, Ukraine

ARTICLE INFO

Article history:
Received 23 May 2014
Received in revised form 29 June 2014
Accepted 9 July 2014
Available online 17 July 2014

Keywords:
Ion exchange
Organic–inorganic ion-exchanger
Standard contact porosimetry
Zirconium hydrophosphate

ABSTRACT

Organic–inorganic ion-exchangers based on gel-like strongly acidic resin, which contain different amount of zirconium hydrophosphate, have been obtained. The samples were investigated using methods of transmission and scanning electron microscopy, standard contact porosimetry, NMR ^{35}P spectroscopy. Nanoparticles of the inorganic constituent (10 nm) are deposited in voids between geld field and in structure defects of the polymer forming aggregates of micron size. These large particles squeeze and stretch pores of the polymer, where $-SO_3$ groups are located, a radius of these pores decreases from 10 nm down to 2 nm. A part of functional groups of the polymer component are excluded from ion exchange due to squeezing of pores, ion exchange properties are determined mainly by the inorganic constituent. Ion exchange capacity of the composites reaches 0.6–1.3 mmol cm^{-3}. These materials sorb preferably Cd^{2+} and Ni^{2+} from solutions, which contain also hardness ions. The highest break-through capacity has been found for the composite with the smallest microporosity of the polymer constituent, this value reaches 80% of total ion-exchange capacity.

1. Introduction

Composites based on ion-exchange resins, which contain metal nanoparticles, are used in catalytic and electrocatalytic processes, particularly for oxygen removal from liquid hydrocarbons [1–3]. Such type of composites is applied to water desalination: silver nanoparticles embedded into resins provide simultaneous disinfection [4]. In this case, the removal of ionic component from water is due to ion exchange ability of the polymer matrix.

A number of organic–inorganic composites, which include inorganic ion-exchangers as a filler, is also known. The composites are characterized by high selectivity towards toxic ions. Modification of polymer ion-exchangers with hydrated oxides of multivalent metals allowed one to obtain materials, which are selective to phosphate [5], arsenite and arsenate [6] anion, some toxic metal cations [7]. Insertion of iron oxide inside resin beads provides their magnetic properties [6,8,9]. Zirconium hydrophosphate (ZHP) embedded into cation-exchange resin enhances its selectivity towards Pb^{2+} [10–14].

The composites based on macroporous resin were obtained [5–14]. However, mobility of sorbed ions through macroporous resins as well as ion-exchange capacity of these materials are lower in a comparison with those for gel-like polymers [15]. It is assumed, that the organic–inorganic ion-exchangers based on this type of resins will provide the most complete removal of toxic ions from weakly concentrated solutions. which contain also hardness ions.

A number of organic–inorganic composites based on gel-like resins containing 8% [16–18] and 2% [19] divinylbenzene has been obtained. The ion-exchangers contained both non-aggregated ZHP nanoparticles and their aggregates [16–19]. However, single nanoparticles were found to block pores of swollen polymer, which contain functional groups [16–18]. This evidently restricts potential possibility of the composites to sorb ions.

Known organic–inorganic ion-exchangers contain mainly aggregates of inorganic constituent [5,7,10–14]. A size of the aggregates is up to several microns, they are evidently located outside nanopores of polymer, where functional groups are placed. Modification of resins with aggregates of inorganic constituent would allow us to reach the most complete removal of toxic ions from diluted solutions. Moreover, extremely small size of inorganic particles is expected to provide high rate of ion exchange.

* Corresponding author. Tel.: +380 444240462; fax: +380 444243070.
E-mail address: dzyazko@hotmail.com (Y.S. Dzyazko).

http://dx.doi.org/10.1016/j.micromeso.2014.07.010
1387-1811/

As found for the materials, which contain both nanoparticles and their aggregates, functional properties of the ion-exchangers (ion-exchange capacity, mobility of sorbed ions, electrical conductivity, swelling, etc) strongly depend on amount of the inorganic constituent [16–19]. The same feature is expected for the ion-exchangers modified by aggregates of nanoparticles. Moreover, the aggregates are assumed to transform porous structure of the polymer. Literature sources contain no information about these problems.

Thus, the aims of the investigation involves synthesis of composite materials based on gel-like polymer containing different amount of inorganic ion-exchanger in a form of aggregated nanoparticles, research of evolution of functional properties of the composites influenced by porous structure of the polymer and chemical composition of the inorganic constituent. Gel-like resin containing 8% divinylbenzene was used as a polymer matrix, the materials of this type are used traditionally for ion exchange processes [20]. ZHP has been chosen as a modifier, since it possesses high selectivity towards heavy metal ions [17,21–24] due to ability of phosphorus-containing functional groups to form complexes with them [21,24].

Sorption of Ni^{2+} and Cd^{2+} cations has been investigated. Cd^{2+} ions are extremely toxic due to their carcinogenic activity [25], Ni^{2+} species are also related to toxic components: they cause pathological effects in humans varying from contact dermatitis to lung fibrosis, cardiovascular and kidney diseases, and even cancer [26]. In owing to this, the content of toxic ions in water and liquid wastes is strictly limited and controlled carefully.

2. Experimental

2.1. Synthesis of organic–inorganic ion-exchangers

Sol of insoluble Zr hydroxocomplexes has been obtained similarly to [27]. As found with a method of laser dynamic light scattering, a size of particles is 4 nm–1.2 μm.

Dowex HCR-S strongly acidic gel-like cation-exchange resin (Dow Chemical) was used as a polymer matrix (marked as *CR*). The resin is based on styrene–divinylbenzene containing $-SO_3H$ groups.

The followings stages were performed: (i) impregnation of a weighed sample of the resin with water for swelling; (ii) filtration; (iii) impregnation of the wet resin with sol for 24 h at 298 K (a ratio of volumes of resin and sol was 1:20); (iv) filtration; (v) treatment of the resin with a 1 M H_3PO_4 solution at 298 K (a ratio of volumes of resin and solution was 1:10); (v) washing with deionized water up to neutral reaction of the effluent; (vi) drying in a desiccator over $CaCl_2$ at room temperature down to constant mass; (vii) treatment of the sample with ultrasound at 30 kHz using *Bandelin* device (*Bandelin electronic*), the treatment was necessary to remove the deposit from outer particle surface; (viii) drying in a desiccator and weighting.

The stages (i)–(viii) were repeated several times. After each modification cycle a sample of the ion-exchanger containing amorphous *ZrPh* was taken for further investigations. Further increase of amount of the inorganic constituent causes to cracking of the beads, no investigations of these samples were provided. In opposite to [10–14] and similarly to [16–19], no organic solvents were used. The samples were marked as (ZHP content, mass%): *CR-1* (31), *CR-2* (43), *CR-3* (49), *CR-4* (52).

Individual *ZHP* was obtained by direct deposition from sol with a H_3PO_4 solution as described above. The ratio of volumes of sol and acid solution was 1:1. The ion-exchangers was washed with deionized water and dried in the desiccator down to constant mass.

2.2. Characterization of samples

Increase of mass was determined by weighting of air-dry resin before and after modification. Swelling was researched according to volumetric measurements of air-dried sample before and after its contact with water [28].

A method of standard contact porosimetry, the principles of which have been described in [29–32], was applied to porosity investigations. The samples were fixed on a paper macroporous support, impregnated with water under vacuum at 353 K and placed between measured and ceramic standards at 0.1 MPa. Further gradual loss of mass of the sample and standards was determined.

Total ion-exchange capacity was found by means of treatment of the samples with a 0.1 M NaOH solution followed by titration of the equilibrium solution with HCl [28]. Each sample was investigated 3 times. The confidence probability of 95% has been chosen. Then the mean value of ion exchange capacity was found for each sample, the standard deviation as well as confidence interval were calculated. The Student coefficient was taken as 4.3 for the chosen confidence probability, since a number of the experiments was 3. The table and plot demonstrate the mean value of the total ion exchange capacity.

SEM images of cross-sections of the particles were obtained by means of a *JEOL JSM 6700 F* scanning electron microscope (*Jeol*). Crushed granules were treated with ultrasound, then a thin layer of platinum was deposited onto the surface at 3 Pa using a *JEOL JFC-1600* Auto fine coater (*Jeol*). TEM images were obtained by means of a *JEOL JEM 1230* transmission electron microscope (*Jeol*).

Zr and P content in the inorganic constituent was determined with analysis of crushed samples using an *X-Supreme8000 XRF* (X-ray fluorescence) spectrometer (*Oxford Instruments*). NMR ^{31}P spectra of the samples, which had been inserted into the ampule with a diameter of 5 mm, were obtained by means of *AVANCE 400* spectrometer (*Bruker*) using single-pulse technique under the accumulation mode at 162 MHz. Chemical shift has been determined relatively to 85% H_3P0_4. The spectra were resolved to Gauss components by means of PeakFit v 4.12 program.

Electrical conductivity of swollen H-forms of the ion-exchangers was measured at 298 K similarly to [17–19]. Deionized water was used as non-conductive medium similarly to [33]. The measurements were carried out by means of an *Autolab* impedance system at 10^{-2}–10^{6} Hz, the conductivity of the bed was determined from frequency spectra of the real part of admittance. The measurements were repeated 3 times for each samples. Statistical treatment of the results were carried out as described above, the mean values of electrical conductivity are given in the plot.

2.3. Ion exchange

The experiments were carried out at 298 K. Fraction of 0.5–0.8 mm of swollen samples was used. The experiments were repeated 3 times for each samples, the plots represent the mean values. The confidential interval was calculated as described in Section 2.2.

Exchange of Ni^{2+}, Cd^{2+} and Ca^{2+} ions on H-forms of the ion-exchangers was investigated under static conditions. Chloride salts were used to prepare one component solutions of different concentrations. The ratio of volumes of ion-exchanger and solution was 0.5 cm^3:100 cm^3. Then the equilibrium solution was separated from the solid and analyzed with an atomic absorption method using a *Pye Unicam SP 9* spectrophotometer (*Philips*).

Kinetics of ion exchange were investigated using a "thin layer" method [34], a scheme of the devise has been given earlier [22]. A one-component solution (5 dm^3) containing 100 mol m^{-3} Cd^{2+}, Ca^{2+} or Ni^{2+} circulated through the ion-exchanger layer (0.5 cm^3)

during 24 h. The contact between the sample and solution was interrupted after pre-determined period, the ion-exchanger was washed with deionized water and regenerated with a 1 M H_2SO_4 solution, the eluate was analyzed as mentioned above.

Ion exchange was also researched under dynamic conditions. Solutions, which contained 0.1 mmol dm^{-3} Ni^{2+} or Cd^{2+}, 1.4 mmol dm^{-3} Ca^{2+} and 0.5 mmol dm^{-3} Mg^{2+} was used. The column diameter was 0.8 cm, the bed volume was 5 cm^3. The multicomponent solution was passed through the bed with a velocity of 0.15 cm^3 s^{-1}. Probes of the effluent were taken regularly and analyzed. The removal degree (*RD*) of species was estimated as $\frac{C_0-C}{C_0}$ (C_0 and C are the concentration at the inlet and outlet of the column, respectively.

3. Results and discussion

3.1. TEM and SEM observation. Location of aggregates in polymer matrix

As known, ion-exchange polymers are structured already at the stage of synthesis: nanosized inhomogeneities are formed as a result of dipole–dipole interaction between functional groups [35–37]. During hydration, these inhomogeneities form gel fields, namely a system of clusters, a radius of which is several nanometers, and channels between them (1–2 nm). The polymer and water in the gel fields are separate phases, in owing to this, the clusters and channels are considered as pores. Functional groups are located inside these pores, which are responsible for ion transport. Voids between the gel fields, where hydrophobic units of polymer chains are placed, are related to meso- and macropores. Additionally, porous structure of gel-like ion exchange materials involves structure defects (up to several microns). Thus, sol particles, a size of which is larger in a comparison with channels, cannot penetrate inside gel fields. ZHP deposition is possible in voids between them and in structure defects.

TEM and SEM images show the inorganic constituent incorporated into the polymer matrix (Fig. 1). A radius of the smallest ZHP particles is ≈10 nm (Fig. 1a). The nanoparticles form blocky aggregates, a radius of which is ≈100 nm (Fig. 1b). The aggregates are constituents of agglomerates of micron size (Fig. 1c). These formations are evidently located in structure defects of the polymer. Small aggregates, a radius of which is ≈50 nm, are placed outside the agglomerates (Fig. 1d). These particles can be located in the voids between gel fields. No single nanoparticles have been found in the polymer.

Thus, in opposite to [10–14], when the macroporous resins were applied, the nanoparticle aggregates have been obtained in a gel-like polymer matrix. In our case, it is possible due to a presence of rather large voids between gel fields and structure defects of micron size. The formation of non-aggregated nanoparticles is impossible, since they are deposited in cluster and channels and stabilized by their walls [17–19]. The deposition in these pores is evidently realized, when a Zr-containing solution is applied for the resin impregnation. Penetration of sol particles, a minimum size of which is 4 nm, into the cluster-channel pore system is impossible dye to steric factor.

3.2. Chemical composition, ion-exchange capacity and swelling

As seen from Table 1, repeated modification procedures caused a growth of mass fraction of the inorganic constituent (*m*). The samples demonstrate an increase of molar ratio of P:Zr with a growth of ZHP content in the polymer matrix.

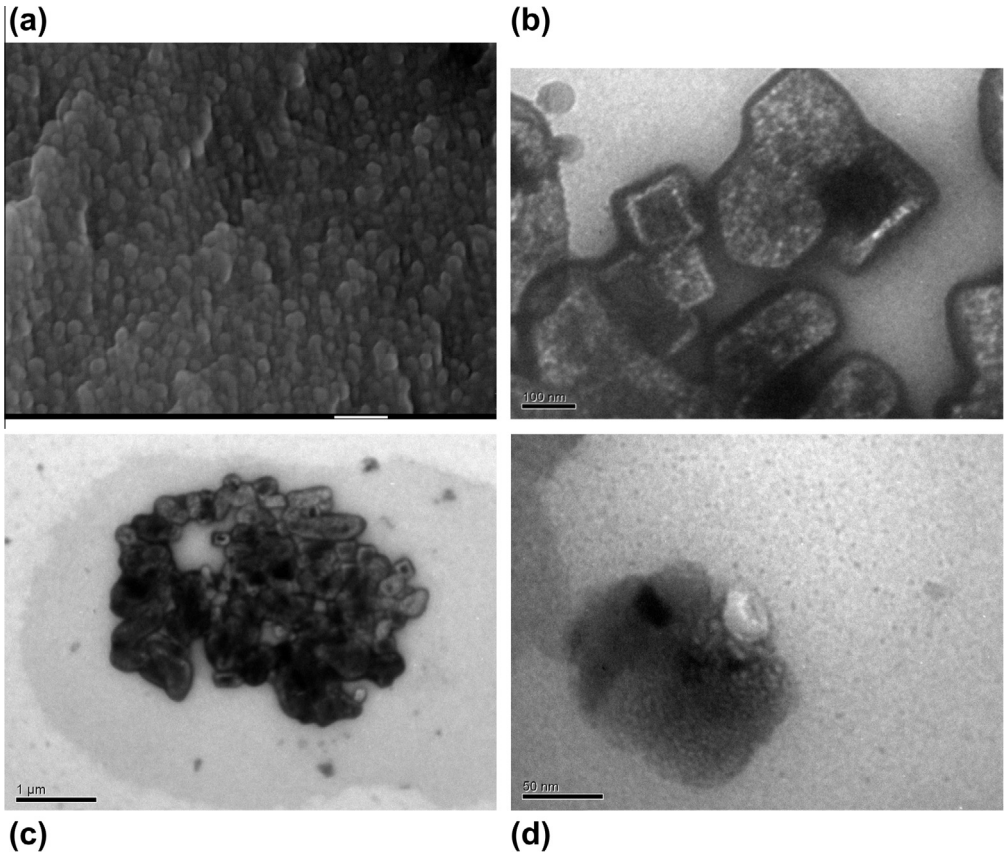

Fig. 1. SEM (a) and TEM (b and c) images of the inorganic constituent embedded into the polymer matrix. Nanoparticles (a), their aggregates (b and d) and agglomerate (c) are visible.

Table 1
Composition of the materials and their ion-exchange capacity.

Sample	m	Molar ratio		$\overline{A}_{Na}$, mmol g^{-1}	$(1-m)\overline{A}_{Na,CR}$, mmol g^{-1}
		P:Zr	$-PO_4H_2$:–$(O_2)PO_4H$		
CR	0	–	–	4.62	4.62
CR-1	0.31	1.80:1	1.15:1	2.33	3.17
CR-2	0.43	1.92:1	1.22:1	1.46	2.62
CR-3	0.49	1.95:1.	1.24:1	1.77	2.34
CR-4	0.52	1.95:1	1.25:1	2.64	2.21
ZHP	1.00	1.44:1	1.05:1	2.60	–

NMR ^{31}P spectroscopy was used for analysis of composition of the inorganic ion-exchanger. Typical spectra, which involve two signals, are given in Fig. 2. Regarding crystalline ZHP containing $(-O)_2PO_2H$ (α-modification) and $-OPO_3H_2$ (γ-modification) groups, the maximum corresponding to hydrophosphate ones is displaced upfield relatively to that for dihydrophosphate groups [38]. The ratio of the signal areas (the integral intensities) corresponds to the molar ratio of functional groups.

As found, dihydrophosphate groups dominates in the inorganic constituent. The molar ratio of $-OPO_3H_2$ and $-(O_2)PO_4H$ groups is higher for the composite materials in a comparison with the inorganic ion-exchanger. Moreover, this ratio decreases with a growth of amount of the inorganic constituent inside the polymer. The literature contains no information regarding the evolution of chemical composition of the inorganic constituent, which is stepwise inserted into the polymer matrix.

Total ion-exchange capacity per mass unit of air-dry materials ($\overline{A}_{Na}$) decreases with a growth of ZHP content (transition from *CR* to *CR-2*). Further increasing in mass fraction of ZHP in the polymer matrix leads to an increase of the $\overline{A}_{Na}$ value. The widest confidence interval was found for the *CR-3* (1.77 ± 0.06 mmol g^{-1}) and *ZHP* (2.60 ± 0.06 mmol g^{-1}). The narrowest interval is attributed to the pristine ion-exchanger (4.62 ± 0.03 mmol g^{-1}). When the particles are located outside pores, which contain functional groups, additivity of ion-exchange capacity should be expected. In this case, the value of $(1-m)\overline{A}_{Na,CR}$, where $\overline{A}_{Na,CR}$ is the capacity of the pristine polymer, should be lower than the $\overline{A}_{Na}$ magnitude. However, $(1-m)\overline{A}_{Na,CR} > \overline{A}_{Na}$ for the *CR-1–CR-3* samples even in spite of the inorganic constituent, which makes a contribution into exchange capacity. It means, a part of $-SO_3H$ groups of the polymer is not involved into ion exchange. Perhaps this causes the lowest ion-exchange capacity for the *CR-2* sample. Improvement of ion-exchange ability (transition from *CR-2* to *CR-4*) is due to influence of ZHP.

The highest swelling is reached for the *CR-2* sample, further increase of the ZHP amount results in a decrease of swelling (Fig. 3). The dependence of exchange capacity per volume unit ($\overline{A}'_{Na}$) *vs* amount of the inorganic constituent shows a minimum for the *CR-2* ion-exchanger. The minimum is due to two factors: minimal capacity per mass unit of this sample on the one hand and its sufficient swelling on the other hand.

Similar results were also found for the ion-exchangers containing both aggregates and single nanoparticles [17–19].

3.3. Porous structure of modified polymer

Since zirconium hydrophosphate looses both free and bonded water at higher temperature, than 353 K, the results of porosimetry measurements are related to polymer. Integral distributions of pore volume (V) are plotted in Fig. 4a. Regarding the pristine ion-exchanger, the V–log r plot demonstrates rapid growth within the interval of log r = 0.5–1 nm. This field is shifted towards lower log r values for modified ion-exchangers. A build-up of the V–log r curves is also observed at log r > 3 nm. The curve intersection with ordinate axe gives a volume of micropores (log $r \leqslant 0$ nm). The highest microporosity has been found for the *CR-1* sample, the *CR-3* ion-exchanger demonstrates the lost volume of micropores.

Fig. 4b illustrates differential distributions of pore volume, the curves are plotted as $\frac{dV}{d(\log r)}$ *vs* log r. Since $\frac{dV}{d(\log r)} = 2.3r\frac{dV}{dr}$, the peak area gives the pore volume.

The curves demonstrate several maxima. Regarding the pristine polymer, the most intensive maximum I (log $r \approx 1$ (nm)) corresponds to pores containing functional groups [16–18,35]. Maximum II (log $r \approx 1.4$ (nm)) can be related to these pores or voids between gel fields. Peak III at log $r \approx 3.2$ (nm) is attributed to structure defects, stripe IV at log $r \approx 4$ (nm) is due to larger structure defects [19] or microcracks on the outer surface of grains. Larger pores are related to voids between grains. The field between

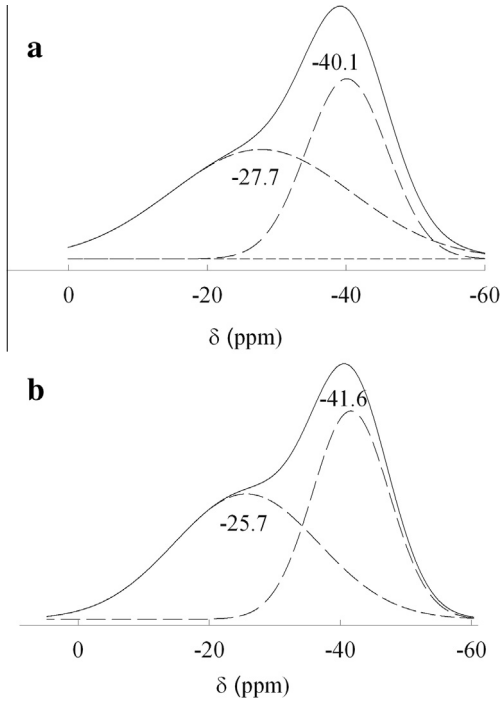

Fig. 2. Typical NMR ^{31}P spectra of individual *ZHP* (a) and organic–inorganic ion-exchanger (b). Experimental (solid lines) and calculated (dashed lines) data are given.

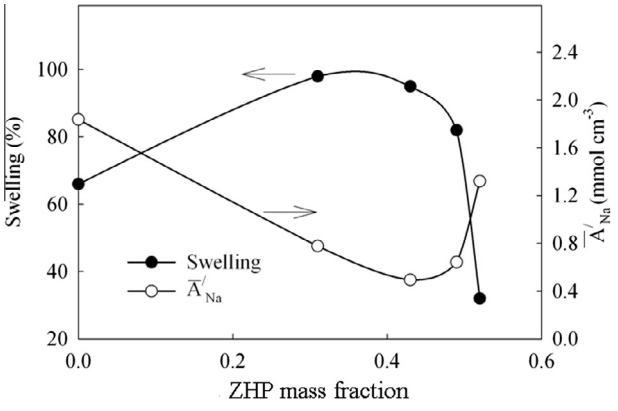

Fig. 3. Swelling and total ion-exchange capacity per volume unit as functions of ZHP amount in the polymer matrix.

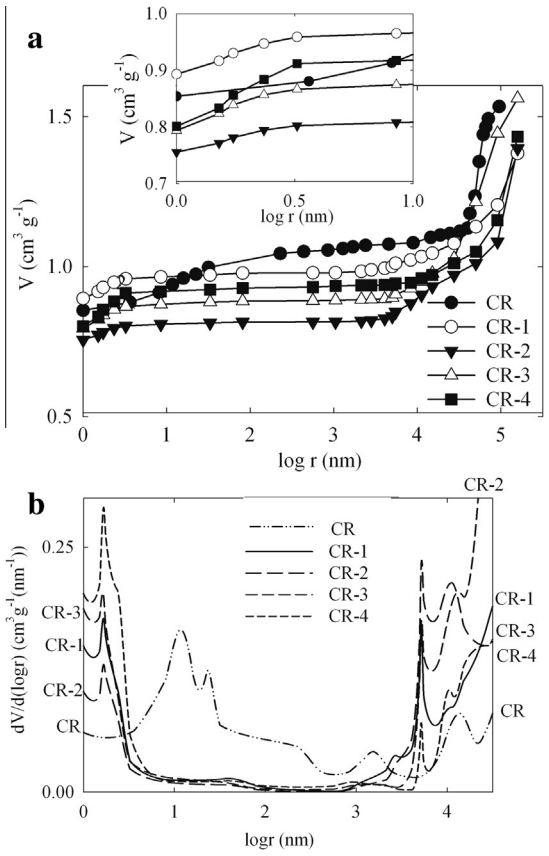

Fig. 4. Integral (a) and differential (b) pore size distributions for the ion-exchangers. Inset of Fig. 4a – integral pore size distribution in a larger scale.

maxima II and III corresponds to voids, which are free from functional groups.

In the case of the *CR-1* sample, maxima I and II are shifted towards lower r values (peak II is visible as a shoulder). Maximum III is split to 3 constituents: peaks: slightly expressed ones at log $r \approx 3.3$ and 3.4 (nm), which are evidently related to pores filled with inorganic constituent, and sharp one at log $r \approx 3.7$ (nm). The last peak probably corresponds to pores, which are free from ZHP. These pores become regular probably due to tension of the polymer.

Decrease of size of pores I and II can be caused by diminishing of swelling pressure due to a decrease of polymer content in the composites. Another reason can be squeezing of these pores by aggregates, which are located outside clusters. As a result, the pore walls are elongated. This is confirmed by integral pore distributions: the volumes of pores in the interval of log $r = 0$–1 (*CR*) and log $r =$ 0–0.5 nm (*CR-1*) are close to each other. Practically similar volume of these pores can be caused only by elongation of their walls.

Edges of large brick-like particles evidently provide small surface of contact with the macropore walls. As a result, pressure on gel-like fields from the side of macropores can be comparable with swelling pressure, which reaches $\approx 1.5 \times 10^7$ Pa for cation-exchanger containing 8% divinylbenzene [34].

Regarding the organic–inorganic ion-exchangers, the area of the maximum I increases in the order: *CR-4* > *CR-3* > *CR-1* > *CR-2*. This order is due to a competition of several factors. The first one is elongation of pore walls influenced by ZHP particles, increase of a distance between functional groups and completion of hydrate shells of counter-ions (increase of swelling, see Fig. 3). Decrease of mass fraction of the polymer in the composites as well as partial unavailability of pores containing functional groups lead to deterioration of swelling.

The area of peaks at log $r > 3$ (nm) increases with an increment of ZHP content (transition from *CR* to *CR-2*) due to stretching of wall of these pores. Further these macropores are partially filled with the inorganic constituent (transition from *CR-2 to CR-4*). The macropores act as microreactors, their enlargement provide deposition of the inorganic ion-exchanger with a higher ratio of dihydrophosphate and hydrophosphate groups in a comparison with individual *ZHP* (see Table 1).

3.3. Electrical conductivity

The impedance measurements were performed for a packed bed, thus, the value of electrical conductivity ($\overline{\kappa}$) depends on resistance at the interface of particle–liquid. Thus, the obtained value allows us to take only qualitative information. Since unloaded forms of the ion-exchangers were investigated, the concentration of H^+ counter-ions per volume unit ($\overline{C}_H$) has to be taken into consideration, $\overline{C}_H \approx \overline{A}'_{Na}$. The $\overline{C}_H$ value includes the concentration of H^+ ions of $-SO_3H$, $-PO_4H_2$ and $-(O_2)PO_4H$ groups. Inorganic particles, which are located outside clusters and channels, make no contribution to conductivity [17,18], it is provided only by a part of $-SO_3H$ groups. These groups are able to dissociate, if they are located in pores filled with water.

The conductivity is seen to be disproportionate to the $\overline{C}_H$ value (Fig. 5). Extrapolation of the linear part of the curve to the *X*-axe gives $\overline{C}_H >> 0$, this confirms exclusion of charge carriers of ZHP groups from proton transport. Other reason of non-linearity of the $\overline{\kappa}$–$\overline{C}_H$ plot can be a change of H^+ mobility due to transformation of porous structure of the polymer, elongation of the walls of transport pores and change of a distance between functional groups.

Very narrow confidence intervals of specific conductivity were found. For instance, the $\overline{\kappa}$ value is 0.103 ± 0.001 for the *CR-1* sample. It should be noted, that the conductivity values for the pristine polymer and *CR-4* are close to each other in spite of partial exclusion of H^+ ions of $-SO_3H$ groups from proton transport. This means higher mobility of species through the composite ion-exchanger in spite of lower size of clusters. This can be caused by an increase of a distance between functional groups. As known, the samples, which contain both aggregated and non-aggregated nanoparticles, demonstrate essential growth of electric conductivity (in 3 times comparing with pristine resin) [17–19]. In our case, we observe no sufficient increase of $\overline{\kappa}$ value due to exclusion of counter-ions of phosphorus-containing groups and partially $-SO_3H$ groups from the ion transport.

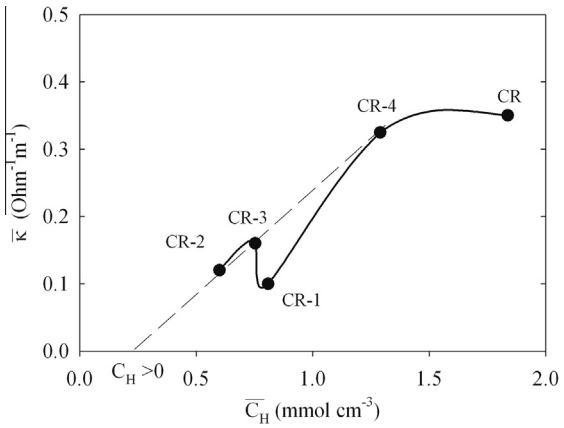

Fig. 5. Conductivity of H-form of the ion-exchangers as a function of concentration of free charge carriers.

3.4. Kinetics of ion exchange

Kinetic curves of $Cd^{2+} \rightarrow H^+$ exchange are shown in Fig. 6 as dependencies of fractional attainment of equilibrium (β, $\beta = \frac{\overline{C}_{Cd,\tau}}{\overline{C}_{Cd,\infty}}$, where $\overline{C}_{Cd,\tau}$ and $\overline{C}_{Cd,\infty}$ are the content of species in ion-exchanger at pre-determined time, τ, and under equilibrium conditions, respectively) against time. The plots for $Ca^{2+} \rightarrow H^+$ and $Ni^{2+} \rightarrow H^+$ look similar, they are not shown. When a solution containing 100 mmol dm^{-3} Cd^{2+} was used, an increase of ion exchange rate was found after interruption and resumption of contact of the ion-exchanger with the liquid similarly to [34]. This indicates diffusion through the solid as a rate-determining step.

Thus, diffusion coefficient, ($\overline{D}$), which corresponds to exchange of cation to H^+, was found from the expression [34]:

$$\overline{D} = 0.03\frac{\overline{r}^2}{\tau_{0.5}}. \quad (1)$$

Here $\overline{r}$ is the particle radius, $t_{0.5}$ is the exchange half-time. The $\overline{D}$ values are plotted in Fig. 7 as functions of mass fraction of ZHP. The confidence intervals for the *CR-1* sample are as follows: $(9.20 \pm 0.24) \times 10^{-13}$ (Ni^{2+}), $(1.83 \pm 0.32) \times 10^{-12}$ (Cd^{2+}), $(2.68 \pm 0.28) \times 10^{-12}$ (Ca^{2+}) $m^2 s^{-1}$. In other words, the diffusion coefficient reduces in the order: $Ca^{2+} > Cd^{2+} > Ni^{2+}$. This order was found also for other samples. The highest diffusion coefficients were found for the pristine ion-exchangers. In this case, high rate of ion transport is provided by clusters, a radius of which is 10 nm. The clusters contain not only bonded, but also free water.

Regarding composite materials, the diffusion of species is realized both through the clusters and channels of the polymer, through macropores towards embedded ZHP particles and inside the particles. Transport pores of the filled polymer contain mainly bonded water, diffusion inside the inorganic particles is complicated by complex formation [24]. These factors slow down diffusion of sorbed species inside grains of the composite ion-exchangers. Similar results were also found for the ion-exchangers containing both non-aggregated and aggregated nanoparticles [16,17].

3.5. Ion exchange under static conditions

Typical isotherms of Cd^{2+} and Ca^{2+} for the pristine polymer, *CR-2* and *CR-4* are given in Fig. 8. The data for other samples as well for $Ni^{2+} \rightarrow H^+$ exchange look similar, they are not represented. For instance, the confidential intervals for the *CR-2* ion-exchanger are: $(2.55 \pm 0.15) \times 10^{-3}$ (the lowest equilibrium concentration of Cd^{2+} in the solution) and 0.10 ± 0.11 (the highest Cd^{2+} concentration) mmol cm^{-3}. The *CR* sample sorbs preferably Ca^{2+}, the composites demonstrate higher uptake of toxic ions. The isotherms have been recalculated in a correspondence to the Langmuir model (Fig. 9) [39]:

$$\frac{C}{\overline{C}} = \frac{1}{\overline{C}_\infty k} + \frac{C}{\overline{C}_\infty} \quad (2)$$

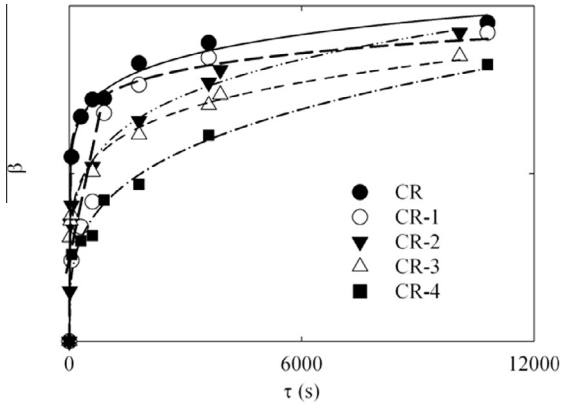

Fig. 6. Kinetics of $Cd^{2+} \rightarrow H^+$ exchange: fractional attainment of equilibrium as a function of time.

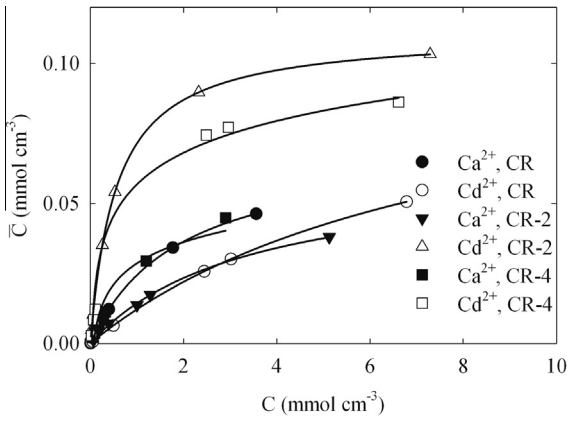

Fig. 8. Isotherms of $Ca^{2+} \rightarrow H^+$ and $Cd^{2+} \rightarrow H^+$ exchange onto polymer and organic–inorganic ion-exchangers.

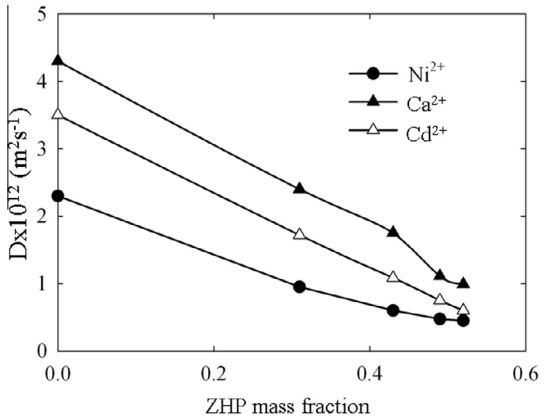

Fig. 7. Diffusion coefficients of Ni^{2+}, Cd^{2+} and Ca^{3+} as functions of ZHP mass fraction in organic–inorganic ion-exchangers.

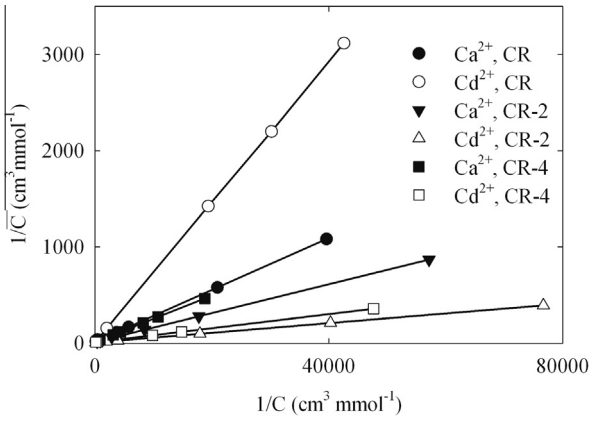

Fig. 9. Langmuir plots of $Ca^{2+} \rightarrow H^+$ and $Cd^{2+} \rightarrow H^+$ exchange onto polymer and organic–inorganic ion-exchangers.

where C is the equilibrium concentration of the solution, $\overline{C}$ is the concentration of species in the ion-exchanger, $\overline{C}_\infty$ is the capacity of a monolayer, k is the constant, which reflects energy of interaction of species with ion-exchanger. The Langmuir constants are shown in Fig. 10. As seen, the highest $\overline{C}_\infty$ and k values were found for the organic–inorganic materials. The plots show maxima, which correspond to the *CR-2* sample. The maxima of the curve can be caused by a competition of several factors. A growth of amount of the inorganic constituent, increase of phosphorus as well as dihydrophosphate groups in ZHP improve sorption of divalent cations, which form complexes with functional groups. On the other hand, partial exclusion of $-SO_3$ groups of the polymer from ion exchange deteriorate sorption. The highest difference between k values for toxic ions and Ca^{2+} was found for the *CR-2* sample, which is characterized by the smallest microporosity of the polymer constituent (see Fig. 4a). This means the smallest contribution of the polymer to selective properties of the composite. Squeezing of walls of mesopores and elongation of their walls can also influence selectivity of the organic–inorganic ion-exchangers.

3.6. Ion exchange under dynamic conditions

The ion-exchangers, excluding *ZHP*, demonstrate high removal degree of Ni^{2+} and Cd^{2+} species (90–99%) from multicomponent solutions, which contained also hardness ions (Fig. 11). However, the break-through capacity towards toxic ions ($\overline{N}_{b,cat}$), total break-through capacity $\overline{C}_{b,t}$ (toward toxic and hardness ions) and the highest relation of concentrations of hardness and toxic ions at the column outlet have been found for the *CR-2* sample (Table 2). These values decrease in the order: *CR-2* > *CR-1* > *CR-3* > *CR-4* > *CR* > *ZHP*. As known, break-through capacity and removal degree of each ionic component depend on selective and kinetic properties of ion-exchangers [34]. Thus, the order is a competitions of two factors: improvement of sorption of toxic ions after modification of the polymer with ZHP and decrease of diffusion coefficient of sorbed ions. The best results for the *CR-2* sample are probably due to their considerable ability to sorb toxic cations. In this case, the $\overline{C}_{b,t}$ value is the most close to the total ion-exchange capacity per volume unit. In opposite to these results, no efficient Cd^{2+} removal was found for organic–inorganic resins, the samples show selectivity only towards Pb^{2+} ions [10–14]. The resins modified only by the aggregates allow us to remove Cd^{2+} and Ni^{2+} ions from a solution containing almost twentyfold excess of hardness ions. The samples containing both non-aggregated and aggregated nanoparticles are able to remove the toxic ions under lower excess of Ca^{2+} and Mg^{2+} [17,19].

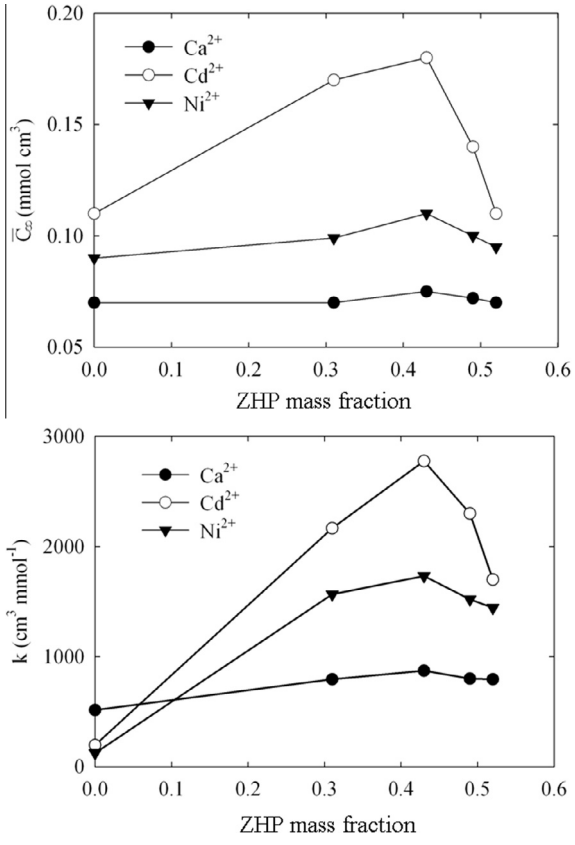

Fig. 10. $\overline{C}_\infty$ (a) and k (b) Langmuir constants as functions of ZHP mass fraction in organic–inorganic ion-exchangers.

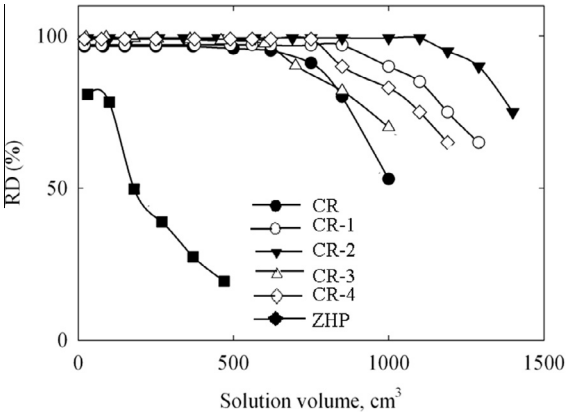

Fig. 11. Removal degree of Cd^{2+} ions from a multicomponent solution as a function of solution volume passed through the column filled with polymer, or organic–inorganic ion-exchangers, or ZHP.

Table 2
Removal of toxic ions from combining solutions.*

Sample	RD_{Cat}, %	$\overline{N}_{br,cat}$, mmol cm^{-3}	$\overline{C}_{br,t}$, mmol cm^{-3}	$\frac{C_{Ca}+C_{Mg}}{N_{Cat}}$,	$\frac{2\overline{C}_{b,t}}{A_{Na}}$
Ni^{2+}					
CR	95	0.011 ± 0.002	0.16 ± 0.02	6	0.17
CR-1	97	0.015 ± 0.004	0.23 ± 0.03	15	0.52
CR-2	99	0.028 ± 0.003	0.24 ± 0.03	27	0.80
CR-3	99	0.013 ± 0.002	0.23 ± 0.02	12	0.72
CR-4	98	0.012 ± 0.002	0.18 ± 0.03	9	0.26
ZHP	81	0.001 ± 0.0008	0.01 ± 0.005	5	0.01
Cd^{2+}					
CR	90	0.012 ± 0.002	0.16 ± 0.04	6	0.17
CR-1	96	0.016 ± 0.005	0.23 ± 0.05	14	0.52
CR-2	99	0.026 ± 0.003	0.24 ± 0.04	26	0.80
CR-3	99	0.014 ± 0.003	0.23 ± 0.04	12	0.72
CR-4	98	0.011 ± 0.002	0.18 ± 0.03	9	0.26
ZHP	75	0.001 ± 0.0006	0.01 ± 0.004	6	0.01

* The data are given for the break-through capacity.

4. Conclusions

Gel-like strongly acidic resin was modified with aggregates of ZHP nanoparticles. A number of composites containing different amount of the inorganic constituent has been obtained. The aggregates, a size of which is from several tens of nanometers to several microns, are evidently located in voids between gel fields and in structure defects. The aggregates stretch these pores providing formation of inorganic ion-exchanger with higher content of phosphorus and dihydrophosphate groups. Large ZHP particles squeeze walls of pores of the polymer, which contain functional

groups, their radius decreases from 10 nm down to 2 nm. Stretching of the pore walls due to their squeezing leads to an increase of swelling and a change of mobility of H^+ ions through the system of transport pores of the polymer. Moreover, $-SO_3$ groups of the polymer are partially excluded from ion exchange. This results in a decrease of total ion-exchange capacity on the one hand and electrical conductivity of H-forms on the other hand. However, this exclusion as well as functional groups of ZHP provide improvement of uptake of Cd^{2+} and Ni^{2+} ions from combining solutions, which contain also hardness ions. The highest Langmuir constant and break-through capacity towards toxic species has been found for the sample with the lowest microporosity of the polymer, which evidently makes the least contribution into uptake of these ions. In this case, sorption behavior of the composites is determined mainly by the inorganic constituent.

Acknowledgements

The work was supported by projects within the framework of programs supported by the Government of Ukraine "Nanotechnologies and nanomaterials" (Grant No. 6.22.1.7), by the National Academy of Science of Ukraine "Problems of stabile development, rational nature management and environmental protection" (Grant No. 30-12) and "Fundamental problems of creation of new materials for chemical industry" (Grant No. 49/12). The work was also supported by the project of the Russian Foundation for Basic Research entitled "Fundamental aspects of deionization of aqueous solutions" (Grant No. 14-03-00082a).

References

[1] M. Basu, T. Pal, in: B.P.S. Chauhan (Ed.), Hybrid Nanomaterials: Synthesis, Characterization and Applications, Wiley, 2011, pp. 23–64.
[2] D. Sengupta, J. Saba, G. De, E. Basu, J. Mater. Chem. A 2 (2014) 3986–3992.
[3] E.V. Zolotukhina, T.A. Kravchenko, Electrochim. Acta 56 (2011) 3597–3604.
[4] B. Domenech, M. Munoz, D.N. Muraviev, J. Macanas, in: A. Mendez-Vilas (Ed.), Microbial Pathogens and Strategies for Combating Them: Science, Technology and Education. Microbial Book Series, vol. 1, Formatex, 2013, pp. 630–640.
[5] L.M. Blaney, S. Cinar, A.K. SenGupta, Water Res. 41 (2007) 1603–1613.
[6] U. Beker, L. Cumbal, D. Duranoglu, Environ. Geochem. Health 32 (2010) 291–296.
[7] S. Sarkar, P.K. Chatterjee, L. Cumbal, A.K. SenGupta, Chem. Eng. J. 166 (2011) 923–931.
[8] M. Pol, A. De, in: L. Merhari (Ed.), Hybrid Nanocomposites for Nanotechnology. Electronic, Optical, Magnetic and Biomedical Applications, Springer, 2009, pp. 455–508.
[9] Y. Lee, J. Rho, B. Jung, J. Appl. Polymer Sci. 89 (2003) 2058–2067.
[10] X. Zhao, L. Lv, B. Pan, W. Zhang, Sh. Zhang, Q. Zhang, Chem. Eng. J. 170 (2011) 381–394.
[11] B. Pan, B. Pan, X. Chen, W. Zhang, X. Zhang, Q. Zhang, Q. Zhang, J. Chen, Water Res. 40 (2006) 2938–2946.
[12] Q.R. Zhang, W. Du, B.C. Pan, B.J. Pan, W.M. Zhang, Q.J. Zhang, Z.W. Xu, Q.X. Zhang, J. Hazard. Mater. 152 (2008) 469–475.
[13] Q. Zhang, P. Jiang, B. Pan, W. Zhang, L. Lv, Ind. Eng. Chem. Res. 48 (2009) 4495–4499.
[14] Q. Zhang, B. Pan, S. Zhang, J. Wang, W. Zhang, L. Lv, J. Nanopart. Res. 13 (2011) 5355–5364.
[15] Yu.S. Dzyazko, V.N. Belyakov, Desalination 162 (2004) 179–189.
[16] Yu.S. Dzyazko, L.N. Ponomareva, Yu.M. Volfkovich, V.E. Sosenkin, Russ. J. Phys. Chem. A 86 (2012) 913–919.
[17] Yu.S. Dzyazko, L.N. Ponomaryova, Yu.M. Volfkovich, V.E. Sosenkin, V.N. Belyakov, Sci. Technol. 48 (2013) 2140–2149.
[18] Yu S. Dzyaz'ko, L.N. Ponomareva, Y.M. Vol'fkovich, V.E. Sosenkin, V.N. Belyakov, Russ. J. Electrochem. 49 (2013) 209–215.
[19] Yu.S. Dzyazko, L.N. Ponomaryova, L.M. Rozhdestvenskaya, S.L. Vasilyuk, V.N. Belyakov, Desalination 342 (2014) 43–51.
[20] B.A. Fil, A.E. Yilmaz, R. Boncukcuoglu, S. Bayar, Bulg. Chem. Commun. 44 (2012) 201–207.
[21] B. Pan, Q. Zhang, W. Du, W. Zhang, B. Pan, Q. Zhang, Z. Xu, Q. Zhang, Water Res. 41 (2007) 3103–3111.
[22] Y.S. Dzyazko, L.M. Rozhdestvenska, A.V. Palchik, F. Lapicque, Sep. Purif. Technol. 45 (2005) 141–146.
[23] Yu S. Dzyazko, L.M. Rozhdestvenska, A.V. Palchik, Rus. J. Appl. Chem. 78 (2005) 414–421.
[24] Yu S. Dzyaz'ko, V.V. Trachevskii, L.M. Rozhdestvenskaya, S.L. Vasilyuk, V.N. Belyakov, Rus. J. Phys. Chem. A 87 (2013) 840–845.
[25] J. Godt, F. Scheidig, Ch. Grosse-Siesttrup, V. Esche, P. Brandenburg, A. Reich, D.A. Groneberg, J. Occupat, Med. Technol. 1 (2006) 22–27.
[26] K.K. Das, S.N. Das, S.A. Dhundasi, Indian J. Med. Res. 128 (2008) 412–425.
[27] Yu S. Dzyazko, A.S. Rudenko, Yu M. Yukhin, A.V. Palchik, V.N. Belyakov, Desalination 342 (2014) 52–60.
[28] M. Marhol, Ion Exchanger in Analytical Chemistry, Academia, 1982.
[29] Yu.M. Volfkovich, V.E. Sosenkin, V.S. Bagotzky, J. Power Sources 195 (2010) 5429–5441.
[30] Yu.M. Volfkovich, V.E. Sosenkin, Russ. Chem. Rev. 81 (2012) 936–959.
[31] Yu.M. Volfkovich, V.S. Bagotzky, V.E. Sosenkin, I.A. Blinov, Colloids Surf. A Physicochem. Eng. Aspects 187–188 (2001) 349–365.
[32] Y.M. Volfkovich, A.V. Sakars, A.A. Volinsky, Int. J. Nanotechnol. 2 (2005) 292–302.
[33] E. Heymann, I.J. O'Donnell, J. Colloid, Science 4 (1949) 395–404.
[34] F. Helfferich, Ion Exchange, Dover, New York, 1995.
[35] N.P. Berezina, N.A. Kononenko, O.A. Dyomina, N.P. Gnusin, Adv. Colloid Interface Sci. 139 (2008) 3–28.
[36] T. Sata, Ion Exchange Membranes: Preparation, Characterization, Modification and Application, Royal Society of Chemistry, 2004.
[37] Y. Tanaka, Ion Exchange Membranes: Fundamentals and Applications, Elsevier, 2007.
[38] I. Nicotera, A. Khalfan, G. Goenaga, T. Zhang, A. Bocarsly, S. Greenbaum, Ionics 14 (2008) 243–253.
[39] N.Z. Misak, React. Polym. 21 (1993) 53–84.